Published online May 31, 2006

2984–2997 *Nucleic Acids Research, 2006, Vol. 34, No. 10*
doi:10.1093/nar/gkl373

New, extended hairpin form of the TAR-2 RNA domain points to the structural polymorphism at the 5′ end of the HIV-2 leader RNA

Katarzyna Pachulska-Wieczorek, Katarzyna J. Purzycka and Ryszard W. Adamiak*

Laboratory of Structural Chemistry of Nucleic Acids, Institute of Bioorganic Chemistry, Polish Academy of Sciences, Noskowskiego 12/14, 61-704 Poznań, Poland

Received February 16, 2006; Revised April 11, 2006; Accepted April 28, 2006

ABSTRACT

The HIV-2 TAR RNA domain (TAR-2) plays a key role in the *trans*-activation of HIV-2 transcription as it is the target for the Tat-2 protein and several cell factors. Here, we show that the TAR-2 domain exists *in vitro* in two global, alternative forms: a new, extended hairpin form with two conformers and the already proposed branched hairpins form. This points strongly to the structural polymorphism of the 5′ end of the HIV-2 leader RNA. The evidence comes from the non-denaturing PAGE mobility assay, 2D structure prediction, enzymatic and Pb^{2+}- or Mg^{2+}-induced RNA cleavages. Existence of the TAR-2 extended form was further proved by the examination of engineered TAR-2 mutants stabilized either in the branched or extended structure. The TAR-2 extended form predominates with an increasing magnesium concentration. Gel retardation assays reveal that both TAR-2 wt and its mutant, unable to form branched structure, bind Tat-2 protein with comparable, high affinity, while RNA hairpins I and II, derived from TAR-2 branched structure model, show much less protein binding. We propose that an internal loop region of the TAR-2 extended hairpin form is a potential Tat-2 binding site.

INTRODUCTION

The 5′-untranslated region (5′-UTR) of the HIV-1 and HIV-2 RNA contains highly structuralized domains playing regulatory role in the viral expression and virion-associated events (1–4). The 5′ end of the HIV-1 and HIV-2 leader RNA is characterized by the presence of the *trans*-activating responsive region (TAR) which appears indispensable for the virus transcriptional regulation (5,6). During initial transcription only a basal level of HIV transcripts is generated to allow synthesis of the *trans*-activator protein Tat (6–9). The transcriptional elongation from the viral long terminal repeat is dramatically enhanced upon TAR RNA interaction with Tat and recruited host cell factors, especially cyclin T1 (10–13). Although most of the data concerning regulation of the viral transcription were accumulated for the HIV-1, similar events are observed (4,9,12) for the less pathogenic HIV-2 (14).

Knowledge of the HIV-1 and HIV-2 TAR RNA structures is crucial not only for the analysis of the *trans*-activation mechanism but also for understanding a dynamic architecture of the whole leader (+1–544) RNA (4) and planning antiviral therapies targeted at RNA and its complexes (15–17). The structure of the 59 nt HIV-1 TAR bulged hairpin (TAR-1) has been well supported by biochemical and biophysical data. Numerous structural studies analysed the functionally important 29 nt TAR-1 RNA in its both free (18,19) and bound forms to such molecules as the argininamide (20) and Tat-related peptides (21,22).

Much less is known about the structure of HIV-2 TAR RNA (TAR-2). In comparison to the TAR-1, a sequence of the TAR-2 is more than doubled in length encompassing +1–123, relative to the transcription start site. Since initial reports from the late 1980s, only the branched, three-hairpins TAR-2 structure was considered (Figure 1A). The model was based on computer analyses (2,23–25) and few structure probing studies (26,27). Contrary to the TAR-1 hairpin containing three-nucleotide bulge, that constitutes the binding site of the viral Tat-1 protein, hairpins I and II of the branched TAR-2 structure each hold pyrimidine dinucleotide bulge and 6 nt apical loop. Much smaller hairpin III contains 5 nt apical loop, has no bulge and does not play any role in Tat-2 binding (6,23). It appears that the apical loop sequence of the TAR-1 is identical to that of the hairpin I of the branched TAR-2. Because of the fact and owing to the spectral difficulties caused by the 123 nt TAR-2 RNA, biophysical studies were concentrated on the NMR structure of the analogue of the TAR-2 hairpin I in its free and the argininamide complexed form (28,29).

*To whom correspondence should be addressed. Tel: +48 61 8528503; Fax: +48 61 8520532; Email: adamiakr@ibch.poznan.pl

This paper is dedicated to Professor Wojciech J. Stec on the occasion of his 65th birthday

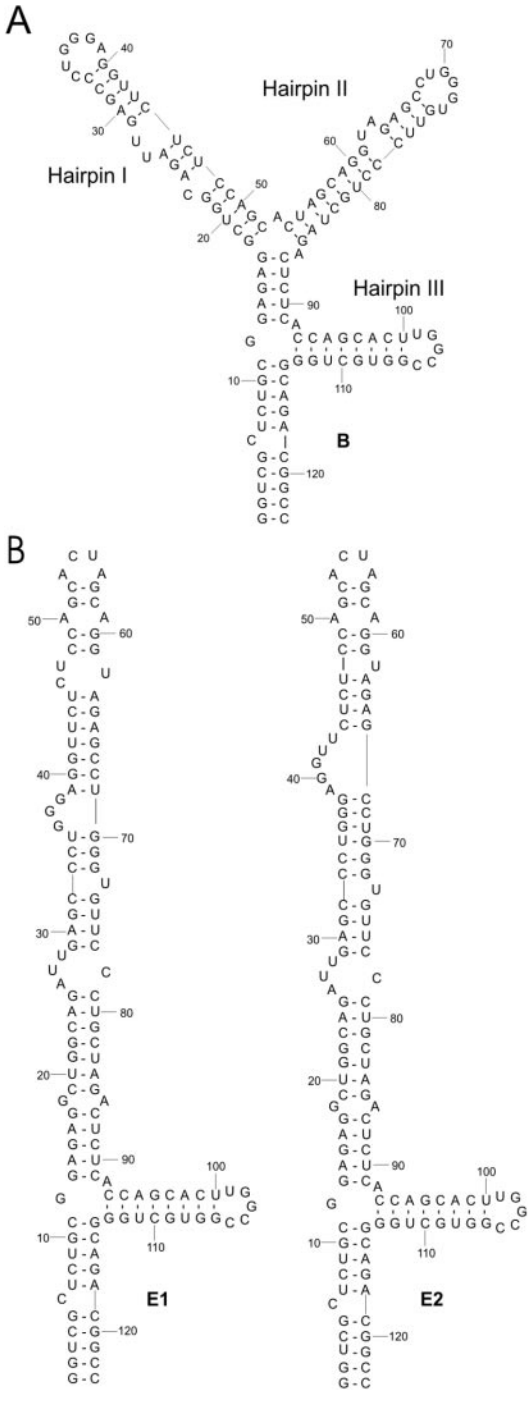

Figure 1. Secondary structure models of the HIV-2 TAR RNA. The models represent the lowest energy solution obtained using the Mfold algorithm and are supported by experimental data. The previously reported branched hairpins form (**A**) stay in equilibrium with the new extended hairpin form represented by two conformers E1 and E2 (**B**). The hairpins I and II of the branched form constitute the arms of the main hairpin of the extended form. Consequently, the branch site between two hairpins becomes an apical loop. The small hairpin, coded III in the branched hairpins structure is identical for all conformers.

As a consequence, our knowledge of the structural details of the TAR-2 RNA interaction with Tat-2 and cellular cofactor cyclin T1 is much less advanced than in the case of TAR-1. In addition, biochemical data concerning TAR-2/Tat-2 binding are often viewed from the HIV-1 perspective, although results of binding and *trans*-activation experiments differ. Apart from homologous binding, Tat-2 protein binds TAR-1 with low affinity and only partially activates HIV-1 LTR, while Tat-1 binds the TAR-1 and TAR-2 RNAs with similar affinity and fully *trans*-activates HIV-1 as well as HIV-2 LTR (6,23,24,30,31). The results relating to the involvement of the TAR-2 branched structure motifs, i.e. hairpins I and II, in Tat-2 binding are often unclear and contradictory. Dinucleotide bulges of both hairpins I (UU) and II (UA) were considered as functionally important (6,27,31). However, the TAR-2 sequence comprising the hairpin I seems to be crucial. It is still unclear whether hairpin I and II act as two functionally independent elements or both regions +18–52 and +54–85 are necessary for Tat-2 binding and efficient *trans*-activation.

Here we propose that the TAR-2 domain exists in two global, alternative forms: in a new, extended hairpin form represented by two conformers and the already proposed three-hairpins branched form (Figure 1). Results of the non-denaturing PAGE mobility assay, 2D structure prediction, enzymatic and Pb^{2+}- or Mg^{2+}-induced RNA cleavages were complemented by analysis of the designed TAR-2 mutants stabilized either in the extended (TAR-2 A21) or branched (TAR-2 B4 and ΔC23) structure, and model oligoribonucleotide hairpins—characteristic motifs of the branched form. Gel shift assays and the argininamide inhibition of Pb^{2+}-induced cleavages were performed to check whether the extended form of TAR-2 has an ability for Tat-2 binding. We hope that the results presented here will shed new light on the structure of the TAR-2 RNA indicating structural polymorphism of the 5′ end of the HIV-2 leader RNA and allow an explanation of some previous data on the TAR-2/Tat-2 interaction.

MATERIALS AND METHODS

Unless indicated otherwise the reagents and materials used in this study were either from Sigma or Aldrich.

RNA synthesis and ^{32}P-labelling

The DNA templates for the *in vitro* transcription were generated by PCR amplification of the plasmid HIV-2 Ψ large (32) containing a T7 promoter directly upstream of the +1 position of the wild-type HIV-2 ROD sequence. Appropriate upstream (p_u) and downstream (p_d) PCR primers were used for template preparation: TAR-2 (p_u gaattctaatacgactcactataggg, p_d ggccgtctgcccagcaccgg), poly(A) (p_u gaattctaatacgactcactatagcacgcttgcttgcttaaaaa, p_d cacacacttaacttgcttct), hairpin I TAR-2 (p_u gaattctaatacgactcactataggctggcagattgagccctgg, p_d gctggagagaaccctggcagctttattaagagg), hairpin II TAR-2 (p_u gaattctaatacgactcactatagctagcaggtagagcctgggt, p_d tctagcagggaac). Templates for mutated transcripts were made by PCR mutagenesis using the appropriate extended upstream primer in which the wild-type TAR-2 sequence was altered to produce desired mutation: TAR-2 A21 (p_u gaattctaatacgactcactatagggtcgctctgcggagaggctagc), TAR-2 B4 (p_u gaattctaatacgactcactatagggtcgctctgcggagaggccggcagattgacccctgggagggtctctccggc) and TAR-2 ΔC23 (p_u gaattctaatacgactcactatagggtcgctctgcggagaggctggagatt). All PCR were performed

in the same conditions using Ambion SuperTaq™ Plus polymerase. The reaction mixture in the total volume of 50 µl contained Ambion PCR buffer with $MgSO_4$ and 50 ng of the DNA template, 100 ng of each primer, 200 µM of each dNTP and 1.25 U of enzyme. PCR thermal conditions were: 95°C for 5 min followed by 30 cycles of 95°C for 1 min, 55°C for 1 min, 72°C for 2 min and then 10 min in 72°C and 10 min in 4°C. The PCR products were precipitated with ethanol and the DNA templates were dissolved in sterile water.

All the RNA transcripts were synthesized with the Ambion T7-MEGAshortscript transcription kit following the manufacturer's protocol. Transcripts were purified and desalted as described earlier (33). The oligoribonucleotides of sequence 21 nt TAR-2 hairpin III and 30 nt hairpin (coded W) used in previous NMR studies (28,29) were obtained by the chemical synthesis using solid-support aided phosphoramidite chemistry and applying the 2′-*O*-TOM protection according to the manufacturer's protocol (Glen Research). Oligomers were purified by preparative gel electrophoresis (19% PAA with 8 M urea), followed by elution and desalting on NAP columns (Amersham Biosciences).

5′ end labelling of RNA molecules was performed using [γ-^{32}P]ATP (ICN) and Ambion KinaseMax kit according to the accompanying protocol. Labelled RNAs were purified by denaturing PAGE, recovered as described previously (33) and quantified using a Beckman LS5000TA scintillation counter.

RNA polyacrylamide gel electrophoresis under non-denaturing conditions

The homogeneity of all RNA molecules was checked on denaturing PAGE. The electrophoresis under non-denaturing conditions was carried out at low, strictly controlled temperature of the gel (4°C) using a Kucharczyk TE DNA Pointer System I equipment or, when indicated, at room temperature. Aliquots of RNAs in sterile water were heated at 90°C for 1 min, cooled to the room temperature and the buffer containing 10 mM Tris–HCl (pH 7.5), 40 mM NaCl and appropriate $MgCl_2$ concentration (0, 0.1, 1, 2.5 and 5 mM) was added prior to the folding (65°C for 10 min, followed by a slow cooling to the room temperature). To stabilize the RNA conformers, the samples were kept on ice for 5 min then 2 µl 30% glycerol or 25% Ficoll with dyes was added and the samples were loaded directly onto the gels (0.5× TB with 0.1% Triton X-100 or 0.5× TBE).

RNA UV melting

Thermal denaturation of the *in vitro* synthesized TAR-2 RNA wt and TAR-2 A21 mutant was monitored at 260 nm on Beckman DU640 spectrophotometer in the temperature range from 25 to 95°C, at the heating rate of 1°C/min with sampling at each 0.5°C. Samples, which contained different RNA concentrations varied over 2-fold range, were dissolved in 150 µl of 50 mM sodium cacodylate buffer (pH 7.2) with no magnesium present or with 1 mM $MgCl_2$. Prior to the measurement, RNAs were incubated at 65°C for 10 min and slowly cooled to 37°C. Non-denaturing gel electrophoresis confirmed the monomeric state of the RNAs. Thermodynamic data were calculated with the MeltWin 3.5 program (34).

In silico 2D RNA structure prediction

Appropriate sequences of HIV-2 and SIV isolates were downloaded from the HIV database (http://hiv-web.lanl.gov) and TAR 2D RNA structures were predicted using two software versions, both based on Zuker's algorithm: RNAstructure PC v. 4.11 and the Mfold web server v. 3.2 (http://www.bioinfo.rpi.edu/applications/mfold/old/rna) applying default settings (35,36). We considered all the secondary structures predicted within 10% of free energy of the most stable variant, subsequently changing window size parameter to generate closely related structures. Design of the appropriate RNA mutants was based on their 2D RNA structure prediction.

Enzymatic RNA structure probing

The limited digestions with nucleases S1 (Fermentas), RNase T1 (Boehringer), RNase V1 (Ambion) and RNase A of the 5′-end-labelled target RNAs (30 000 c.p.m. per sample) were performed in a buffer containing 10 mM Tris–HCl pH 7.2, 40 mM NaCl, 8 µM carrier tRNA (Ambion) and 5 mM $MgCl_2$. Prior to the reactions RNAs were refolded by heating at 90°C for 1 min in reaction buffer and slowly cooling to room temperature. The renatured RNAs were incubated for 10 min at room temperature or at 37°C (S1) with increasing concentration of appropriate enzyme: S1 (0.5, 0.75, 1 U), T1 (0.2, 0.3, 0.4 U), V1 (0.01, 0.005, 0.0025 U), A (0.1, 0.05, 0.01 ng). The reactions were terminated by adding an equal volume of stop buffer (8 M urea, 20 mM EDTA, 0.02% xylene cyanol and 0.02% bromophenol blue) and freezing on dry ice. Similar experiments were also carried out at constant single strand-specific enzymes concentrations (T1, 0.4 U; S1, 1 U and A, 0.1 ng) with varying concentration of $MgCl_2$ (0–10 mM).

Chemical RNA structure probing

For the chemical structure probing with the diethylpyrocarbonate (DEPC) in non-denaturing conditions (10 mM Tris–HCl pH 7.2, 40 mM NaCl and 5 mM $MgCl_2$), the target 5′ end labelled RNAs (50 000 c.p.m) were refolded and incubated with 0.5 µl DEPC for 5, 25 or 45 min at 37°C. Samples were ethanol precipitated twice and treated with 10 µl of 1 M aniline–acetate buffer (pH 4.5) according to the standard protocol (37). Before electrophoresis, the RNAs were dissolved in 5 µl of sterile water and the equal volume of formamide with tracking dyes was added.

For the RNA cleavage with hydroxyl radicals generated by the Fe(II)-EDTA, 5′ end labelled RNA (100 000 c.p.m.) was dissolved in buffer containing 50 mM Tris–HCl (pH 7.5), 1 mM $MgCl_2$ and 5 mM DTT. Subsequently, 1 µl of freshly prepared 50 mM ammonium iron(II) sulfate hexahydrate solution and 1 µl 20 mM EDTA (pH 8.0) were added. The reactions were incubated at room temperature for 5, 10 and 15 min. After reaction, 10 µl of formamide with tracking dyes was added and the samples were loaded directly on the denaturing gel.

Pb^{2+} and Mg^{2+}- ion-induced RNA cleavages

Prior to the Pb^{2+} ion-induced cleavage reaction, RNA transcripts (30 000 c.p.m.) were subjected to the refolding procedure as described above using reaction buffer: 10 mM Tris–HCl (pH 7.2), 40 mM NaCl, 8 μM carrier tRNA and 10 mM $MgCl_2$. Afterwards, freshly prepared $Pb(OAc)_2$ solution was added to the final concentration of 0.25, 0.5, 1 and 2 mM and the reaction mixtures were incubated for 15 min at room temperature. For Mg^{2+} ion-induced cleavage reaction, RNA transcripts were dissolved in solution containing 40 mM NaCl, 8 μM carrier tRNA and 0.025 mM EDTA, heated at 90°C for 1 min, cooled to the room temperature and the Tris–HCl (pH 8.5) was added to the final concentration of 10 mM. Subsequently, $MgCl_2$ was added to reach 0.25, 0.5, 1 or 2 mM concentration. The reaction mixtures were incubated for 15 h at 37°C. All reactions were quenched by the addition of an equal volume of the stop buffer.

For competitive inhibition of Pb^{2+}-induced RNA cleavage, the 5′ end labelled RNAs (30 000 c.p.m.) were refolded as described above for the Pb^{2+} cleavage reaction, but the buffer contained no $MgCl_2$. The reactions were performed at a constant 2 mM concentration of $Pb(OAc)_2$ and in the presence of increasing concentrations of the competitor, i.e. argininamide dihydrochloride (1, 2, 5, 10, 20, 30, 40 and 50 mM) or $MgCl_2$ (1, 2, 5, 10, 20, 30, 40 and 50 mM), at the room temperature for 15 min. All the reactions were quenched by the addition of an equal volume of the stop buffer.

All the products of the nuclease digestions and chemical cleavages were analysed by denaturing PAGE (8 M urea, acrylamide/bisacrylamide in the ratio 29:1) in 1× TBE (100 mM Tris, 100 mM boric acid and 2.5 mM EDTA). Different percentages of the gels were used (8, 10 and 15%) depending on RNA length. In order to assign the RNA cleavage sites the reaction products were subjected to the electrophoresis along with the products of alkaline RNA hydrolysis (formamide with 3 mM $MgCl_2$ at 100°C for 20 min) and limited T1 nuclease digestion (0.2 U, 50 mM sodium citrate, pH 5.3 and 7 M urea at 55°C for 10 min) of the same RNA.

Preparation of the HIV-2 Tat protein

Tat-2 was expressed in *Escherichia coli* BL21—Codon Plus (DE3)–RIL cells (Stratagene) as the glutathione S-transferase (GST) fusion protein. After expression, the fusion protein was purified and cleaved with the thrombin enzyme as described earlier (38). Tat-2 protein was stored in a buffer containing 50 mM Tris–HCl (pH 7.9), 20 mM KCl and 1 mM DTT at 4°C. Under these conditions, protein shows high RNA binding activity for ∼1 month.

TAR-2 RNA/Tat-2 gel retardation assay

RNA–protein complex formation was carried out in the buffer (10 μl) containing 50 mM Tris–HCl (pH 8.0), 20 mM KCl, 100 mM DTT, 0.1% Triton X-100 and 0.5 μg carrier RNA. After incubation at 0°C for 10 min, samples were mixed with 2 μl of 25% (w/v) Ficoll with dyes and loaded directly on non-denaturing polyacrylamide gel (acrylamide/bisacrylamide 75:1) containing 0.5× TB with 0.1% Triton X-100. The PAGE was carried out at low, strictly controlled temperature of the gel (4°C). Depending on RNA length a different percentage of the gels was used (6 or 10%).

Results from all PAGE experiments with radiolabelled RNAs presented in this study were visualized and quantitatively analysed using phosphorimaging screens and a Typhoon 8600 Imager with ImageQuant software (Molecular Dynamics). On all figures representative results are presented, but they were derived from at least three independent experiments.

RESULTS AND DISCUSSION

Electrophoretic RNA mobility points to the existence of two global TAR-2 forms; magnesium dependence

Studies presented in this article were initiated by a surprising observation that the TAR-2 RNA showed a tendency to migrate as two bands (Figure 2A), but only if the non-denaturing PAGE was carried out under strictly controlled temperature of the gel, 4°C. Such a characteristic pattern was observed despite different denaturation/renaturation protocols tested. Finally folding conditions presented in the Materials and Methods were used in order to get a full coherence with previously reported results concerning the TAR-2 structure (27,39). Existence of two bands was taken as an indication that TAR-2 can adopt at least two structural forms. It was strongly supported by the

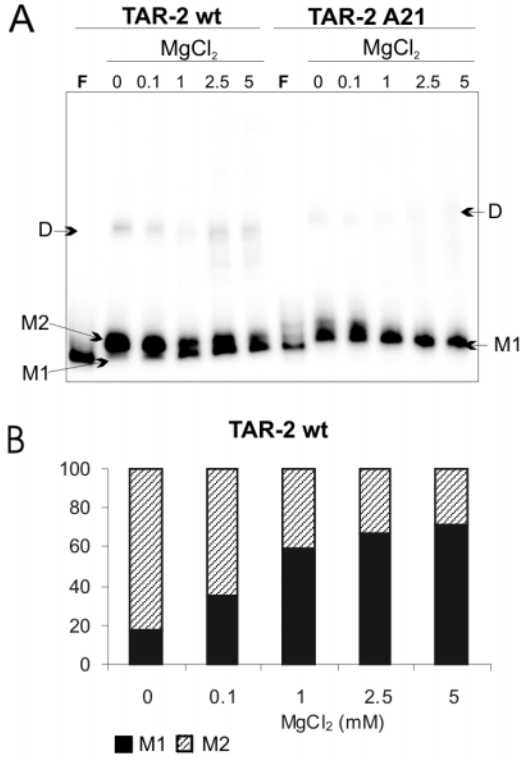

Figure 2. Magnesium-dependent mobility of TAR-2 RNA and TAR-2 A21 mutant on non-denaturing PAGE. **(A)** 123 nt TAR-2 wt and its A21 mutant. (**B**) Plotting of the phoshoimager quantification of the TAR-2 wt fast and slow migrating bands ratio, averaged from several experiments. Alternatively folded monomeric RNAs are indicated as M and the dimers as D. Lanes F correspond to formamide-denatured control samples. $MgCl_2$ concentrations (mM) are indicated above the respective lanes. The samples were analysed on a 6% non-denaturing 0.5× TB with 0.1% Triton X-100 gels. Similar results were obtained in 0.5× TBE buffer without Triton X-100 (Figure S1A).

in silico 2D structure prediction (see below). Based on a commonly accepted assumption that the branched RNA conformers migrate slower than extended, we postulate that the slow mobility band corresponds to the TAR-2 branched form and the fast mobility band corresponds to the extended form. Nearly identical mobility of both forms made their clear-cut separation difficult. Until now all reports showed the presence of only one band for the 123 nt TAR-2 RNA transcripts under non-denaturing PAGE conditions (6,11,31,39). The following conditions were found optimal for their separation: the acrylamide/bisacrylamide ratio (75:1), the constant current parameters (30 mA, 350 V), addition of 0.1% of Triton X-100 to the electrophoresis buffer, low RNA amounts subjected to the analysis and, most importantly, strictly controlled temperature (4°C) of the gel (compare Figure 2A and Figure S1A).

Interestingly, the balance between two global TAR-2 forms depended on the magnesium concentration starting from its low range, characteristic of the *in vivo* conditions. When the folding of RNA was carried out in the buffer with no $MgCl_2$ present or under low 0.1 mM $MgCl_2$ concentration, the branched TAR-2 form was the predominant one. A nearly equal amount of both TAR-2 forms was observed at 1 mM $MgCl_2$. The increasing magnesium ions concentration (from 0.1 to 5 mM $MgCl_2$) increased the proportion of the TAR-2 extended form, which was the major detectable monomeric form above ~2.5 mM (Figure 2B).

To test whether the faster migrating band is related to the extended form of the TAR-2 RNA we have constructed the TAR-2 A21 mutant (substitution G21A) which, as was indicated by the Mfold software, can adopt the extended form but not the branched hairpins form (Figure S2A). Indeed, the TAR-2 A21 mutant exhibited mobility consistent with TAR-2 wt, however migrated just behind a faster migrating band of the TAR-2 wt. Moreover, TAR-2 mutants stabilized in the branched form (coded B4 and ΔC23, see below) were not conclusive in assigning bands to the particular forms, most probably due to the point mutations. We found this explanation justified since it was shown that the RNA structure alteration by a single nucleotide substitution might cause differences in electrophoretic mobility under non-denaturing conditions (40). In our case, this effect was observed only at low temperature of the gel. When the electrophoresis was carried out at room temperature, TAR-2 wt and A21, B4, ΔC23 mutants exhibited nearly the same mobility (Figure S1C). Most probably the TAR-2 A21 mutant required magnesium for its proper folding; under non-denaturing PAGE conditions, the A21 mutant migrated as a sharp band only if folded with 1 mM or higher $MgCl_2$ (Figure 2A). This effect was not owing to the different salt concentrations in the analysed samples, since the poly(A) domain migrated independently on $MgCl_2$ concentration, as a sharp band with the same mobility in each lane (Figure S1B).

The TAR-2 wt showed single ultraviolet transition under low monovalent salt conditions (4). Using the same conditions, we have observed the same profile not only for TAR-2 wt but also for TAR-2 A21 mutant. An addition of $MgCl_2$ to the final concentration of 1 mM caused the increase of the T_m from 60.1 to 76.5°C and from 62.8 to 77.7°C for the TAR-2 wt and TAR-2 A21 mutant, respectively. It indicated only structure stabilization by magnesium ions. Analysis of thermodynamic data (Table S1) revealed that the difference in the free energies between TAR-2 wt and TAR-2 A21 mutant was quite high in the buffer without magnesium; when 1 mM of $MgCl_2$ was present their free energies became nearly the same. Free energy changes observed for TAR-2 wt suggest that in the presence of magnesium a conformational change is taking place and TAR-2 wt exhibits structural properties closer to the TAR-2 A21 mutant. This was in accord with non-denaturing PAGE results.

In silico 2D TAR-2 RNA structure prediction

For the TAR RNA domain of the HIV-2 ROD isolate, the Mfold generated two well-ordered global structure models as the most stable variants, one of which was the new extended hairpin form of the lowest energy (coded E1), and the other was the well-known branched form with three hairpins (coded B) (Figure 1). It should be emphasized that nucleotide residues involved in the TAR-2/Tat-2 interaction assigned to the hairpin I bulge of the branched structure model remain single-stranded in the extended hairpin model and are located in the internal loop. However, from the dinucleotide bulge of hairpin II only U62 remains single stranded in the model of the extended form. It is interesting that although there was a significant difference in the global structure between these two forms, their free energy was very similar: $\Delta G = -65.4$ kcal/mol and $\Delta G = -66.7$ kcal/mol for branched and extended form of the TAR-2 ROD isolate, respectively. As the enzymatic structure probing (see below) showed structural flexibility in the G-rich region (G36G37G38A-39G40G41) of the TAR-2, we have returned to the *in silico* search for closely related structures. Interestingly, Mfold generated, apart from irregular forms, the second extended hairpin model (coded E2) of $\Delta G = -66.4$ kcal/mol, which fulfilled experimental data. A three-nucleotide bulge (G36G37G38) appeared characteristic of a more stable conformer E1 while, a five-nucleotide bulge (A39G40G-41U42U43) was predicted for E2.

It is interesting to investigate whether the tendency to adopt the extended form is seen for other HIV-2 and also SIV isolates, as the HIV-2 is genetically more closely related to SIV than to HIV-1 (14). For that purpose the 2D structure prediction of the TAR domain was carried out on all available, comparable in length, nucleic acids sequences of HIV-2 and SIV isolates. For all analysed HIV-2 and SIV isolates the extended form of the TAR domain was predicted as the most stable variant, with the one exception for SIV-STM. The phylogenetic comparison of the TAR RNA sequences of analysed HIV-2 and SIV isolates revealed small number of sequence variations (Figure S3) and these did not exclude the formation of the branched and extended global forms. However, we cannot rule out that the extended form may be specific for some clades.

The Mfold-assisted *in silico* search was used also to design the appropriate RNA transcripts which would fold in either the branched or the extended form exclusively. Unfortunately, the stabilization of the TAR-2 branched hairpins form with preserved, functionally important, bulged and apical loop regions would require too many in-stem substitutions to exclude potential equilibration with the energetically favoured extended hairpin form. Interestingly, only single

point mutation (i.e. either G21A or G18U) was enough to generate exclusively the extended hairpin form. Transcript of the TAR-2 A21 mutant (G21A) as the best potential mimic of the extended form was prepared and examined experimentally. As in the case of TAR-2 wt the designed TAR-2 A21 mutant was represented by two conformers (Figure S2A).

However, during the revision stage, owing to the suggestion of the anonymous referee, we have returned to the above mentioned, but put aside, models of the branched TAR-2 form. Two mutants which show the highest tendency to form the branched structure were chosen. Even though, we have searched for variants with the minimal sequence changes, the first model, coded B4, needed as many as four base substitutions located in both stems of the first TAR-2 hairpin: U20C, A50G, G31C and U42G (Figure S2B). Second model, coded ΔC23, was based on the deletion of a single-bulged cytidine residue located in the lower stem of the first TAR-2 hairpin (Figure S2C). TAR-2 mutated B4 and ΔC23 transcripts were prepared and examined experimentally.

Enzymatic and chemical TAR-2 RNA structure probing

The RNA structure probing was based on partial digestions with specific nucleases, Pb^{2+} and Mg^{2+}-induced cleavages, and on chemical modifications. Since we dealt with a balance of two global TAR-2 RNA forms, many nucleotide residues exhibited properties typical for single-stranded regions despite of their assignment to the different motifs i.e. bulges, apical loops or internal loops. The balance between TAR-2 conformers depended strongly on magnesium concentration. This prompted us to search for characteristic, preferably magnesium-dependent cuts, which would allow assigning them either to the structure of the branched or extended form. Comparison of the probing data of the full-length TAR-2 wt with its A21, B4, ΔC23 mutants and oligoribonucleotides comprising defined motifs of the branched structure model, i.e. hairpin I (+18–52) and II (+54–85), appeared to be crucial. The TAR-2 A21 mutant was used as a mimic of the TAR-2 RNA molecule in its extended form and B4 and ΔC23 mutants as the models of the branched TAR-2 form.

Enzymatic cleavages. Single-strand specific nucleases namely T1, S1, A and double-strand specific ribonuclease V1 were used. Within the TAR-2 wt considered as a branched structure, the apical loop of hairpin I was cleaved very strongly, whereas the apical loop of the hairpin II was resistant to enzymes (Figure 3A and C, and Figure S4). It was surprising, since the sequence of six-residue apical loops of hairpin I and II is almost identical. The G36, G37 and G38 residues formerly assigned to the apical loop of hairpin I were highly accessible to T1; in particular, G36 was cleaved very strongly. Our results concerning hairpin II region were consistent with earlier observation of the lack of the RNase T1 specific cleavages at G70, G71 and G72 residues (3,26) but they were at variance with other data, collected at high enzyme concentration (27). Although, the lack of G70-G72 cleavages for the TAR-2 wt domain was previously discussed in a view of the long-distance interactions of those residues with the region (+189–191) located in between poly(A) and PBS domains (3), that explanation found no support in our data as they were obtained for the isolated 123 nt TAR-2 wt domain. Two completely different cleavage patterns for these two loops do not fit the TAR-2 branched hairpins model (Figure 3A and C). On the contrary, they can be easily explained if the extended hairpin form is considered; residues G70, G71 and G72 are base-paired whereas G36, G37 and G38 show tendency to the bulge formation. In addition, the lack of G70-G72 cleavages in the A21 mutated molecule (Figure 3B and Figure S5) strongly supported our conclusion that these nucleotide residues are base paired in the extended form of the TAR-2 wt RNA. Additional confirmation was obtained from the analysis of the mutants B4 and ΔC23 for which cleavages at the second apical loop of the branched form were clearly seen (Figure S6).

The ribonuclease T1 digestions appeared to be very informative not only in allocating specific cuts to the extended structure but also in demonstrating its conformational flexibility reflected within the G-rich region—G36G37G38A39G40G41. Despite great care about the reproducibility of the ribonuclease T1 digestions, undertaken in numerous experiments, we have observed two characteristic gel patterns for that region (Figure 3D). The first one, reflecting higher accessibility of G36, G37 and G38 residues, corresponded mainly to the branched structure and extended conformer E1. The second pattern, more often observed, with the strongest cleavages at G40 and G41, could not be explained on the basis of both TAR-2, the branched and E1 structures, since these residues form stable G–C pairs. It should be emphasised that those two T1 cleavage patterns, characteristic of G-rich regions, were also observed for the TAR-2 A21 mutant. Those experimental results found full explanation in the *in silico* prediction which pointed to the second extended hairpin conformer E2 and E2-A21, for both TAR-2 wt and A21 mutant, respectively.

Results obtained for the full-length TAR-2 RNA cleavages were confronted with those from the enzymatic structure probing of 35 and 32 nt oligoribonucleotides of a sequence of hairpins I and II of the branched structure model, respectively (Figure S7). In contrast to the full-length TAR-2 wt and its A21 mutant transcripts, residues G40 and G41 (numbering as for full-length transcripts) of the isolated hairpin I, base-paired like in the TAR-2 branched structure model, were not cleaved with RNase T1. It should be underlined that for the full-length TAR-2 B4 and ΔC23 mutants, a total lack of T1 cleavages at G40 and G41 residues was also observed (Figure 3E). It convinced us that cleavages at those residues are characteristic only for the TAR-2 conformer E2.

Moreover, the cleavage at U35, located in the apical loop of hairpin I, with ribonuclease A was much stronger than for both full-length TAR-2 and its A21 mutant. In the extended hairpin conformers U35 is involved in G–U base pairing and placed on the edge of the bulge (E1) or within stem (E2). Strong cleavages at the second apical loop of the B4 and ΔC23 mutants and at the loop of isolated hairpin II, with single-strand specific enzymes, unobserved in the wild-type full-length TAR-2 transcript, supported existence of the extended form of the TAR-2 in which residues U69–G72 are base-paired. Moreover, the isolated hairpin II showed very strong specific cleavages at G70 and G71 induced by the hydroxyl radicals (Figure S7B).

Very strong cuts at U55 with RNase A and nuclease S1 were characteristic of both wild type and A21 mutant

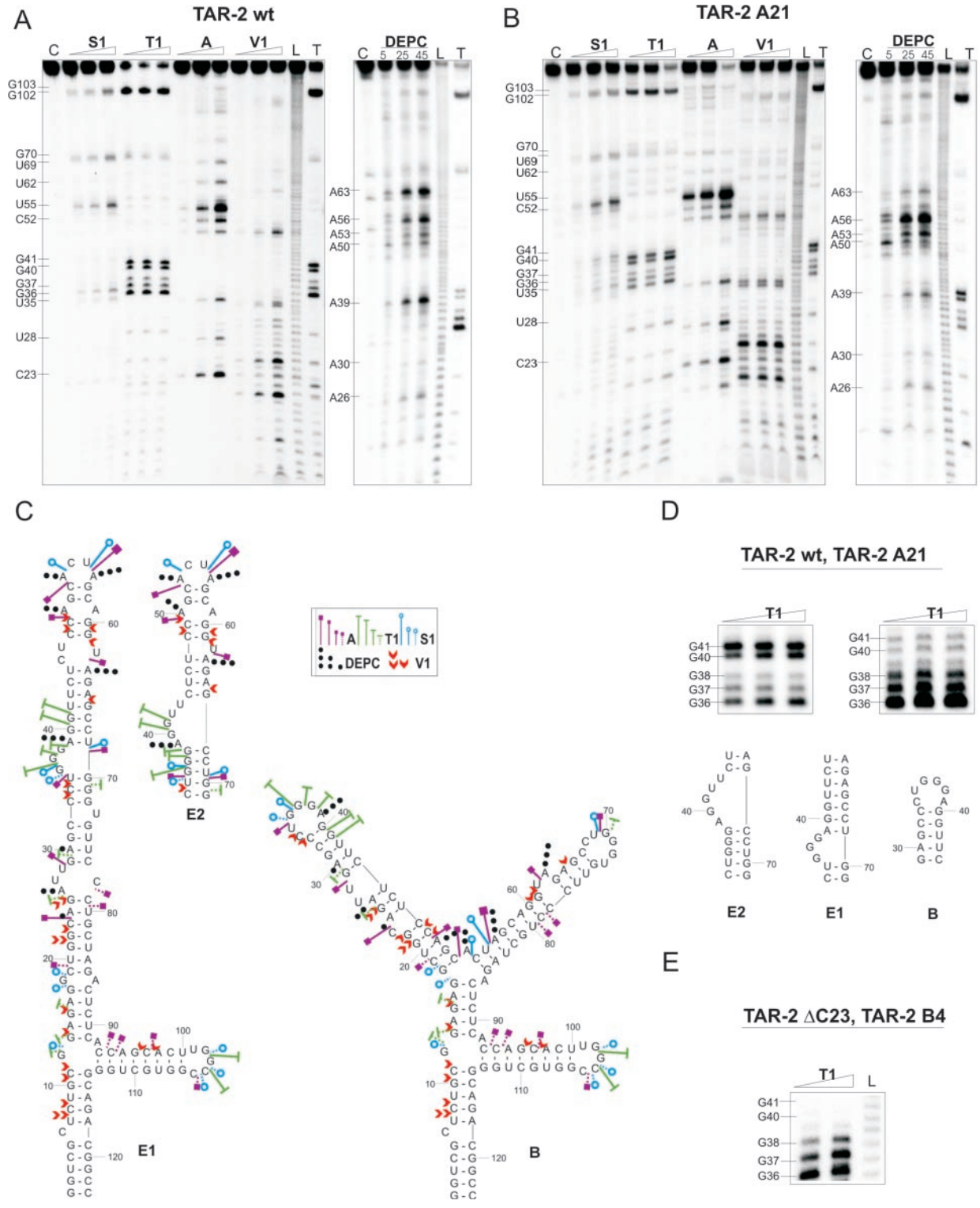

Figure 3. Secondary structure probing of HIV-2 TAR RNA. The RNA was treated with selected single-strand specific enzymes (S1, T1, A), DEPC and double-strand specific RNase V1. (**A**) Cleavage patterns obtained for the 5′ end labelled TAR-2 wt transcript. Lanes C represent control sample with untreated RNA; lanes L, formamide ladder; lanes T, limited hydrolysis with RNase T1. (**B**) Cleavage patterns obtained for the 5′ end labelled TAR-2 A21 mutant transcript. (**C**) A summary of the enzymatic cleavages and chemical modifications data for the TAR-2 wt RNA viewed on the secondary structure models (E1, E2 and B). For clarity, only the top part of the E2 conformer that differs from E1 is shown. Sites and intensities of cleavages with the respective reagents are indicated by symbols (see inset); the size of a symbol corresponds to the relative cleavage intensity. The weakest cleavages are not indicated. (**D**) Two different RNase T1 cleavage patterns observed for the particular G-rich region of both TAR-2 wt and A21 mutant along with respective secondary structure motifs. Both patterns point to the mixture of TAR-2 forms; the right pattern is consistent mostly with one of the extended (E1) and with the branched (B) structure models; the most often observed left pattern represents predominantly the second extended conformer E2. (**E**) RNase T1 cleavage pattern obtained for the TAR-2 B4 and ΔC23 mutants stabilized in the branched (B) form.

TAR-2 RNAs (Figure 3 and Figure S5). For the TAR-2 wt, U55 cleavage increased with a magnesium concentration above 1 mM, i.e. conditions leading to the prevalence of the extended form (Figure S4). The aforementioned results were in favour of the existence of the extended hairpin conformers E1 and E2 where the U55 is placed in the apical loop. Although, the accessibility of residues U55–G57 to single strand-specific enzymes was observed earlier (11,27), their occurrence was explained in a view of the branched structure model, as caused by the tertiary structure interactions that would prevent stable base-pairing of those nucleotide residues (27). For the TAR-2 B4 and ΔC23 mutants, cleavages at residues close to the branch site and formulating the lower part of the second hairpin stem were also observed, although much less intensive that for the TAR-2 wt and A21 mutant (Figure S6). The presence of cleavages in TAR-2 transcripts stabilized in either extended or branched form supports both explanations.

Two dinucleotide bulges U27U28 and U62A63 are characteristic of the TAR-2 branched structure model. In the absence of magnesium, strong cleavages at U27 and U28 residues with ribonuclease A were observed for TAR-2 wt (Figure S4). Addition of $MgCl_2$ led to the inhibition of those cleavages to the level noticed for the TAR-2 A21 mutant. This was not observed for the 35 nt hairpin I (data not shown). Those facts, electrophoretic mobility and presented below results of Mg^{2+}-induced RNA cleavages suggest that the TAR-2 wt undergoes magnesium-dependent conformational change; bulged U27 and U28 are rearranged to the different structural motif—an internal loop of the extended hairpin form. Independently of the magnesium concentration, residues U62 and A63, within both TAR-2 wt and its A21 mutant, were cleaved weaker than U27 and U28 (Figure 3 and Figure S5). Results on full-length TAR-2 wt and A21 transcripts were in contrast to both isolated hairpins I and II for which strong cleavages of comparable intensities were observed at respective bulge regions (Figure S7). One point remains unanswered, i.e. the presence of strong cleavage at C23 not only in the TAR-2 wt, as expected, but also in TAR-2 A21 mutant.

It should be underlined that from all enzyme cleavages studied, only digestions with ribonuclease A responded specifically to the magnesium concentration, which was taken as an advantage in assigning cuts representative to either branched or extended form. In case of other enzymes, cleavage intensities increased proportionally with a higher concentration of magnesium within the range studied (0–10 mM, data not shown).

Similar to single-strand specific enzymes, the V1 induced cleavages occurred for TAR-2 wt and its A21 mutant at the same positions and especially strong cuts were observed at U7, G21 (A21 for A21 mutant) and G25 that are predicted to be base paired in both TAR-2 structure models (Figure 3).

Chemical structure probing with the DEPC. was performed to assign location of the key single-stranded adenosine residues to the different structural motifs of the branched and extended TAR-2 forms. Low reactivity of N7 site of the adenosine residues was ascribed to its involvement in base pairing and stacking interactions (37,41). In the TAR-2 wt transcript only few adenosine residues underwent DEPC modification; residues A39, A56 and A63 appeared as hyper reactive (Figure 3A and C). A39 is present in an apical loop in the branched hairpins structure model. In the TAR-2 A21 mutant, lower intensity of A39 modification was observed (Figure 3B and Figure S5), indicating stacking of that residue in the conformer E1 while in the E2 it stays unpaired. The A56 residue, highly reactive in TAR-2 wt, showed also the highest reactivity in the A21 mutant. This residue in the extended form is placed within apical loop of the main hairpin whereas in the branched one it is in the middle of the helix. Modification at A56 pointed strongly to extended hairpin conformers, whereas reaction at the A63 residue, weakly modified in the TAR-2 A21 mutant, pointed to the branched form of TAR-2 wt. Results of RNA modification by DEPC were in agreement with other data showing alternative structures of the TAR-2 wt.

Pb^{2+} ions-induced RNA cleavages. Metal ions promoted RNA cleavages are very sensitive tools used to map single-stranded regions and metal ions coordination sites in the RNA structure (42,43). Two dinucleotide bulges U27U28 and U62A63, characteristic of the TAR-2 branched structure model, were recognized by Pb^{2+} ions in a completely different manner. The region related to the first bulge showed the strongest cleavages of all, while that of the second bulge was cleaved much weaker and only at U62 (Figure 4A and C). Obtained cleavage patterns fit well into the extended structure of TAR-2 where these two sites are differently arranged: U27 and U28 are placed in an internal loop, the U62 is unpaired and A63 is base paired. Similar cleavage pattern for U27, U28, U62 and A63 residues was observed for the TAR-2 A21 mutant (Figure 4B and Figure S8). In contrast to the full-length TAR-2 wt, strong Pb^{2+} -induced cleavages were observed at both bulge sites of isolated hairpins I and II, including A63 residue (Figure S7). For both TAR-2 RNA wt and its A21 mutant, and consistent with the enzymatic structure probing, nucleotide residues expected to form the first apical loop (+34–39) within the branched hairpins structure were hydrolysed stronger with Pb^{2+} ions than those from the second apical loop (+68–73) (Figure 4A and C, and Figure S8). This is due to the tendency of residues +34–39 to form the bulge and its vicinity within extended form while nucleotide residues +68–72 are base-paired in both conformers E1 and E2. This explanation found strong support in previous studies (44) which showed that in most cases bulges and internal loops were more readily cleaved with Pb^{2+} ions than apical loops. Furthermore, the apical loop residues of isolated hairpin I were cleaved weaker than in the full-length TAR-2 wt (compare Figure 4A and Figure S7). Residue U55, strongly cleaved with single-strand specific enzymes was moderately cleaved with Pb^{2+} ions for both TAR-2 wt and A21 mutant RNAs. This observation pointed to U55 positioning in the apical loop of extended hairpin conformers rather than disturbing base pairing in this region by tertiary interactions, as was proposed earlier (27). Moreover, U69 residue strongly cleaved in the isolated hairpin II, (Figure S7B) was cleaved only weakly in the wild TAR-2 transcript, which indicated its involvement in the base pairing as in the extended structure model.

Mg^{2+}ions-induced RNA cleavages and potential magnesium binding sites. As was shown by the gel electrophoresis under

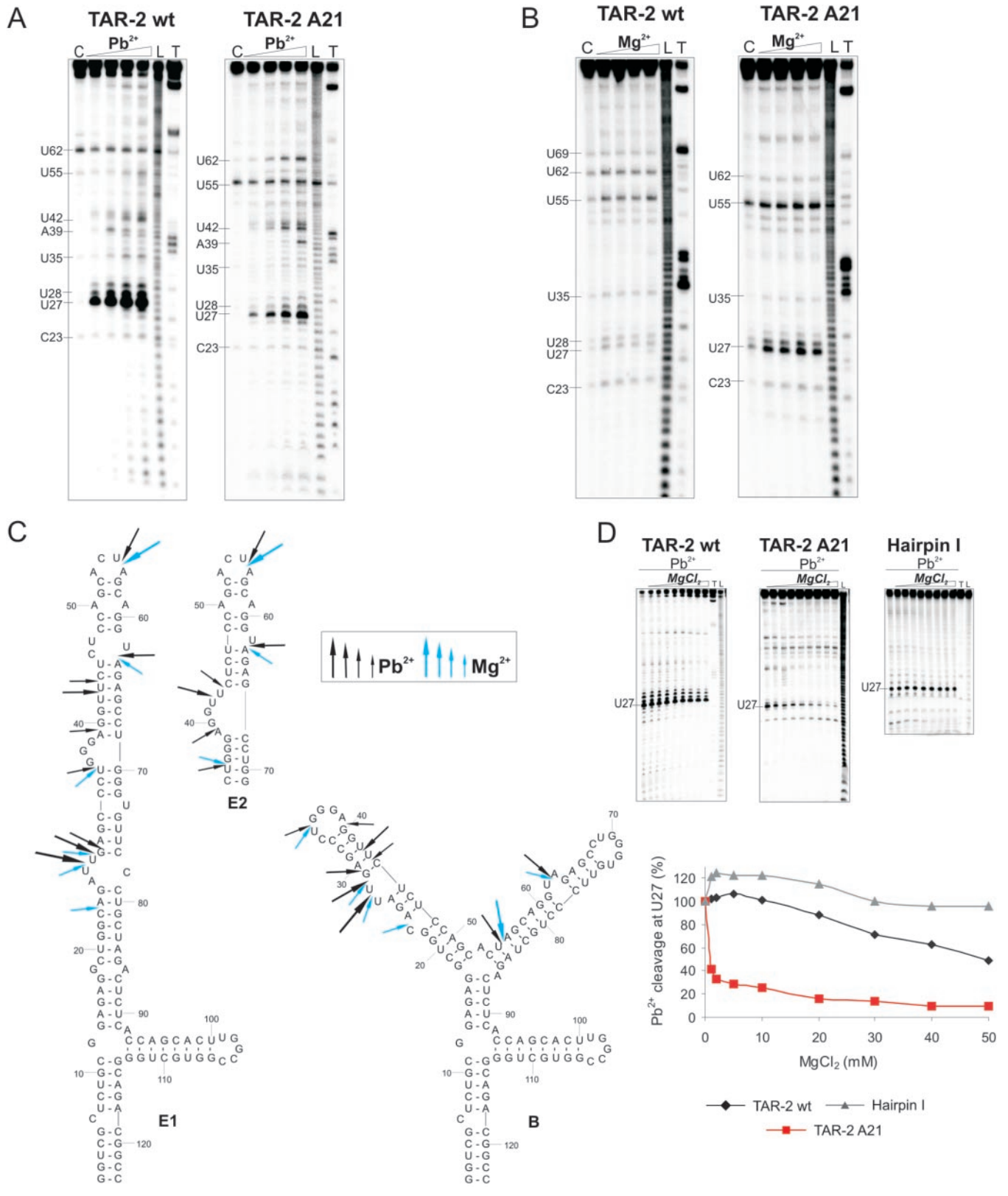

Figure 4. Metal ions-induced TAR-2 RNA structure probing. (**A**) Pb^{2+}-induced RNA cleavage of TAR-2 wt and TAR-2 A21 mutant. (**B**) Mg^{2+}-induced RNA cleavage of TAR-2 wt and TAR-2 A21 mutant. Lane C represents control sample with untreated RNA; lane L, formamide ladder; lane T, limited hydrolysis with RNase T1. (**C**) A summary of the Pb^{2+}- and Mg^{2+}-ions induced RNA cleavages of the TAR-2 wt, viewed on the secondary structure models (B, E1, E2). For clarity, only the top part of the E2 conformer that differs from E1 is shown. Sites and intensities of cleavages are indicated by arrows (see insert); size of symbols corresponds to the relative cleavage intensity. The weakest cleavages are not indicated. (**D**) The comparison of the inhibitory effect of Mg^{2+} on Pb^{2+}-induced cleavages at U27 position of TAR-2 wt, TAR-2 A21 mutant and TAR-2 isolated hairpin I.

non-denaturing conditions and thermodynamic data, Mg^{2+} ions are crucial for changing the balance between two TAR-2 RNA forms and for the stabilization of the extended structure. To get deeper insight in the involvement of Mg^{2+} ions in governing the TAR-2 conformational properties, the experiments of Mg^{2+} ions-promoted cleavages and Mg^{2+} ions competitive inhibition of Pb^{2+}-specific RNA cleavages were performed (Figure 4 and Figure S8). It should be recalled here that conditions applied for the cleavage reaction with Mg^{2+} (low-$MgCl_2$ concentration, pH 8.5, 37°C, 15 h) were quite different from those for Pb^{2+}-promoted RNA cleavages due to much higher pK_a value of corresponding metal ion hydrate (43).

Although Mg^{2+}-induced cleavages at the U27 and U28 residues were observed for TAR-2 wt and A21 mutant, they appeared especially strong for the TAR-2 A21 mutant suggesting magnesium ion binding in that region of the extended hairpin structure (Figure 4). This assumption was supported by a strong Mg^{2+} inhibition of the Pb^{2+}-specific cleavage at U27 position of TAR-2 A21 mutant, the effect noticeable starting from low-$MgCl_2$ concentration (Figure 4D).

For the TAR-2 wt the inhibition was weaker and pronounced only at higher $MgCl_2$ concentration whereas for the isolated hairpin I no cleavage inhibition at U27 was observed. Not surprisingly, taking under consideration equilibrium between the branched and extended forms of the full-length TAR-2 in low-$MgCl_2$ concentration, those cleavages and Mg^{2+}-inhibited Pb^{2+} cleavages for the TAR-2 RNA wt were less intensive. These results provided further evidence that the extended form of TAR-2 binds Mg^{2+} ions preferably at internal loop site.

Does the extended hairpin form of the TAR-2 RNA bind Tat-2 protein?

TAR-2/Tat-2 gel shift assays. To answer the above question, the Tat-2 binding to the 123 nt TAR-2 RNA, its A21, B4, ΔC23 mutants and isolated hairpins I, II and III, representing motifs of the branched structure model, was analysed using gel shift assays. Most importantly, it appeared that Tat-2 was able to bind full-length TAR-2 wt and TAR-2 A21 mutant with the same affinity (Figure 5). For both transcripts, formation of the array of discrete complexes at lower protein concentrations was observed; those bands disappeared with an increasing amount of the protein and a strong broad band of the complex (or complexes) was observed. Similar

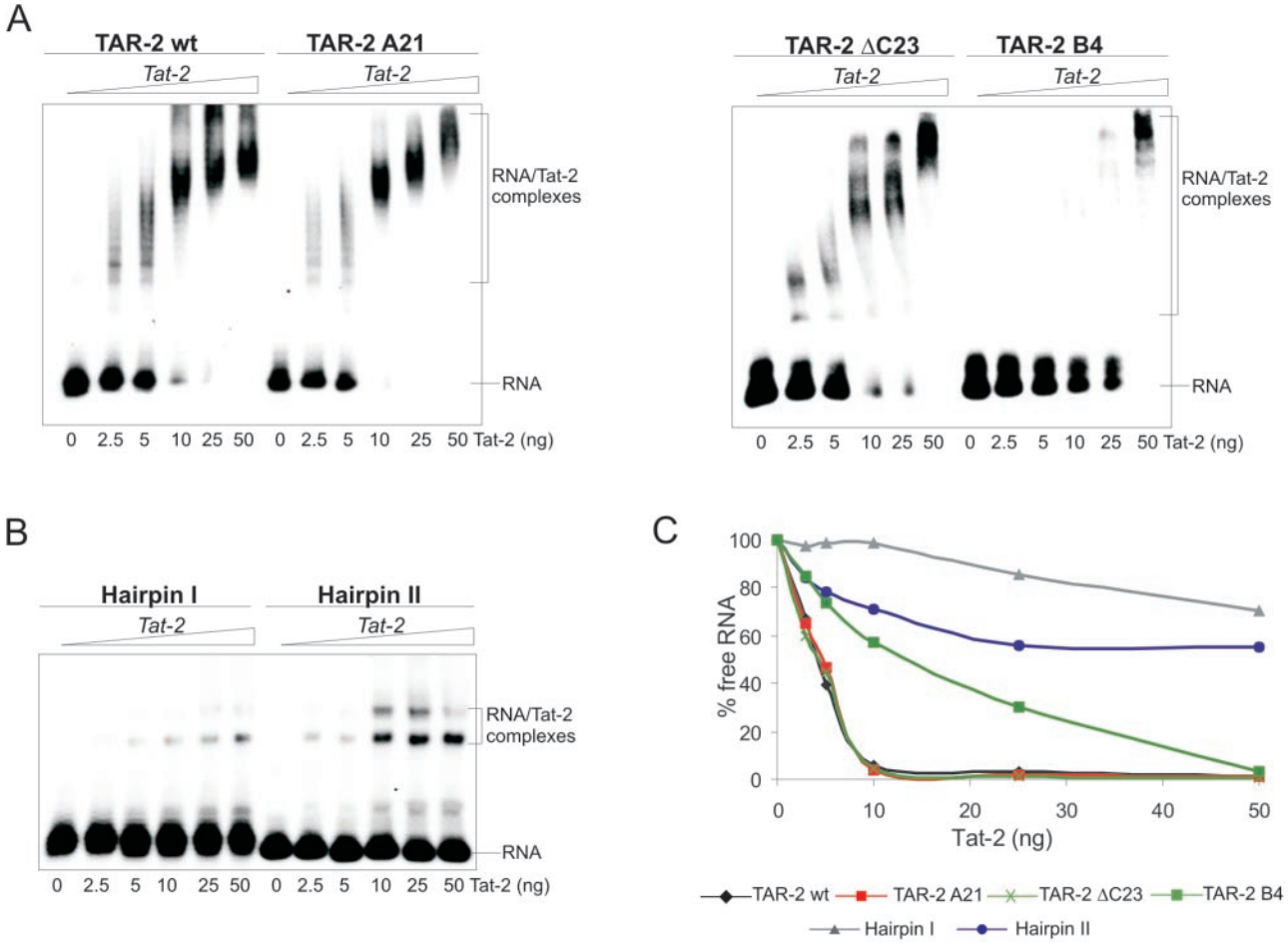

Figure 5. Gel shift assays of the Tat-2 binding to: (**A**) TAR-2 wt and its mutants, (**B**) isolated hairpins I and II corresponding to the TAR-2 RNA branched structure. (**C**) Panel C shows the plot of the Tat-2 binding affinity observed for the TAR-2 wt, TAR-2 mutants and isolated hairpins I and II. Amounts of the Tat-2 protein (ng per reaction) are indicated below their respective lanes.

gel patterns were previously reported for the TAR-2 wt (6,27). High-binding affinity of the Tat-2 to the TAR-2 A21 mutant strongly indicated that the structural motifs other than dinucleotide bulges, not present in the extended conformers, should be considered as the Tat-2 binding sites.

Since all former reports on Tat-2 binding were focused on the branched TAR-2 structure, one would expect that the analysis of B4 and ΔC23 mutants will deliver conclusive results on the involvement of the branched form in the protein association. It appeared that the B4 mutant shows very low Tat-2 binding. An initial excitement about that result was tempered by the fact that TAR-2 ΔC23 mutant showed Tat-2 binding affinity comparable with both, TAR-2 wt and its A21 mutant (Figure 5). At this stage we do not want to draw any conclusions about potential biological relevance of the fact that one of the mutants stabilized in branched form binds Tat-2 with significantly lower affinity than wild TAR-2. This shows us how careful one should be in manipulating a native RNA structure and reveal that too many substitutions in the stem motifs (mutant B4) may have a great impact on the TAR-2 properties (see below on the argininamide binding to the hairpin W).

Interesting results were delivered from the analysis of isolated hairpins I (+18–52) and II (+54–85) which were expected to serve as good models of the single binding site for the Tat-2 within the TAR-2 branched form. It appears that isolated hairpins I and II were bound by Tat-2 with significantly lower affinity than that observed for the full-length TAR-2 wt and its A21 and ΔC23 mutants (Figure 5). As expected, no Tat-2 binding was observed for 21 nt hairpin III of TAR-2 (Figure S9). Surprisingly, the Tat-2 formed more tight complexes with the isolated hairpin II than with the hairpin I. Above facts suggested that the nucleotide residues +18–85 of the full-length TAR-2 wt, covering the sequence of both hairpins I and II, are important not only for the architecture of the extended conformers but also for Tat-2 binding *in vitro*. This was in accord with the reports showing that for effective *trans*-activation the HIV-2 leader RNA required an additional sequence +54–85 (region of the hairpin II) (2,24); deletion of the hairpin II sequence reduced the *in vivo* response to Tat-2 by 3-fold (30).

Competitive inhibition of Pb^{2+}-induced RNA cleavages by argininamide. Since the argininamide tends to induce similar structural changes at the TAR-1 bulge site as Tat-1 protein, the Tat binding was often simplified to the interaction with argininamide (20,28,29,45). We have shown earlier that binding of argininamide to the bulge region of TAR-1 RNA caused inhibition of Pb^{2+}-induced cleavages (33). The same approach was used here to find potential argininamide binding sites in the TAR-2 structure. The 60 nt RNA of the poly(A) sequence was used as a reference molecule since that domain showed no Tat-2 binding (Figure S10A). Increasing the concentration of the argininamide had no influence on Pb^{2+}-induced cleavage of poly(A) RNA (Figure S10B).

Dinucleotide bulges U27U28 and U62A63 were proposed as Tat-2 binding sites of the TAR-2 branched hairpins structure (27). For the TAR-2 wt, an increasing concentration of the argininamide strongly inhibited Pb^{2+}-induced cleavage at U27 residue (Figure 6). Interestingly, the cleavage at U62 was strongly enhanced. Such differences in the argininamide binding are difficult to explain if one considers the similarity of both potential Tat-2 binding sites within the branched form. They rather indicate that only the region related to the first bulge of the TAR-2 branched structure model has the ability for Tat-2 binding. On the other hand, in the TAR-2 extended conformers, residues U27 and U62 are placed in different structural motifs. One of them is composed of the unpaired U27 residue and adjacent base pairs G29-C77 and A30-U76, a base arrangement closely resembling that of the TAR-1 and hairpin W (see below) bulge regions, proved to be important for the argininamide and, putatively, Tat interactions (19,21,28,29). As far as the second motif is concerned we can not fully explain the argininamide influence on the Pb^{2+}-induced cleavage at the unpaired U62 residue, placed in very different structural environment within the branched (B) and extended conformers E1 and E2. Instead of the enhancement seen for the TAR-2 wt, nearly no effect was observed for the TAR-2 A21 mutant (Figure 6B). Currently, we cannot exclude sequential bindings of argininamide.

At this stage we have turned to the analysis of isolated hairpins I and II—motifs of the branched structure model. Contrary to the argininamide inhibited Pb^{2+}-induced cleavage at U27 of the 123 nt TAR-2 wt, no inhibition was observed for the isolated 35 nt hairpin I. This result was surprising in a view of the reported NMR structure of the complex between so-called first TAR-2 hairpin and the argininamide (28,29). An inspection of the bulged hairpin chosen for these studies showed that its sequence is not exactly that of the wild-type TAR-2 but instead it is a chimera of the TAR-1 hairpin structure where typical UCU bulge was replaced by UU, characteristic of the TAR-2 hairpin I. Since both TAR-1 and TAR-2 first hairpin have the same apical loop sequence, thus the helical stems make the difference (see above on the Tat-2 binding affinity of the B4 mutant). That hairpin (coded hairpin W, Figure 6), in contrast to the isolated hairpin I used here, revealed very strong argininamide inhibition of Pb^{2+}-induced cleavages. The lack of argininamide induced inhibition at U27 of isolated hairpin I was also consistent with its very low Tat-2 binding affinity described above. Clear differences in the argininamide inhibition of Pb^{2+}-induced cleavage were also observed for the U62 residue of the 123 nt TAR-2 wt and isolated 32 nt RNA hairpin II. An increasing argininamide concentration caused an inhibition for the isolated hairpin II. In accord, the formation of the tight Tat-2 complexes with isolated hairpin II was observed during gel shifts experiments. Above results convinced us that the approach we have applied is very sensitive to the structure of analysed RNA and can be used to probe RNA sites of argininamide binding, all in relation to arginine-rich proteins such the Tat.

Indication that the internal loop with U27 and adjacent residues constitute the argininamide binding site in the TAR-2 extended form and most probably the part of the Tat-2 binding site was confirmed by the analysis of the TAR-2 A21 mutant adopting only extended hairpin structure. For TAR-2 A21 mutant, which earlier showed high Tat-2 binding affinity, a strong argininamide inhibition of Pb^{2+} induced cleavage at U27 position was observed. Although future biophysical studies are needed to reveal specificity of TAR-2/Tat-2 interaction,

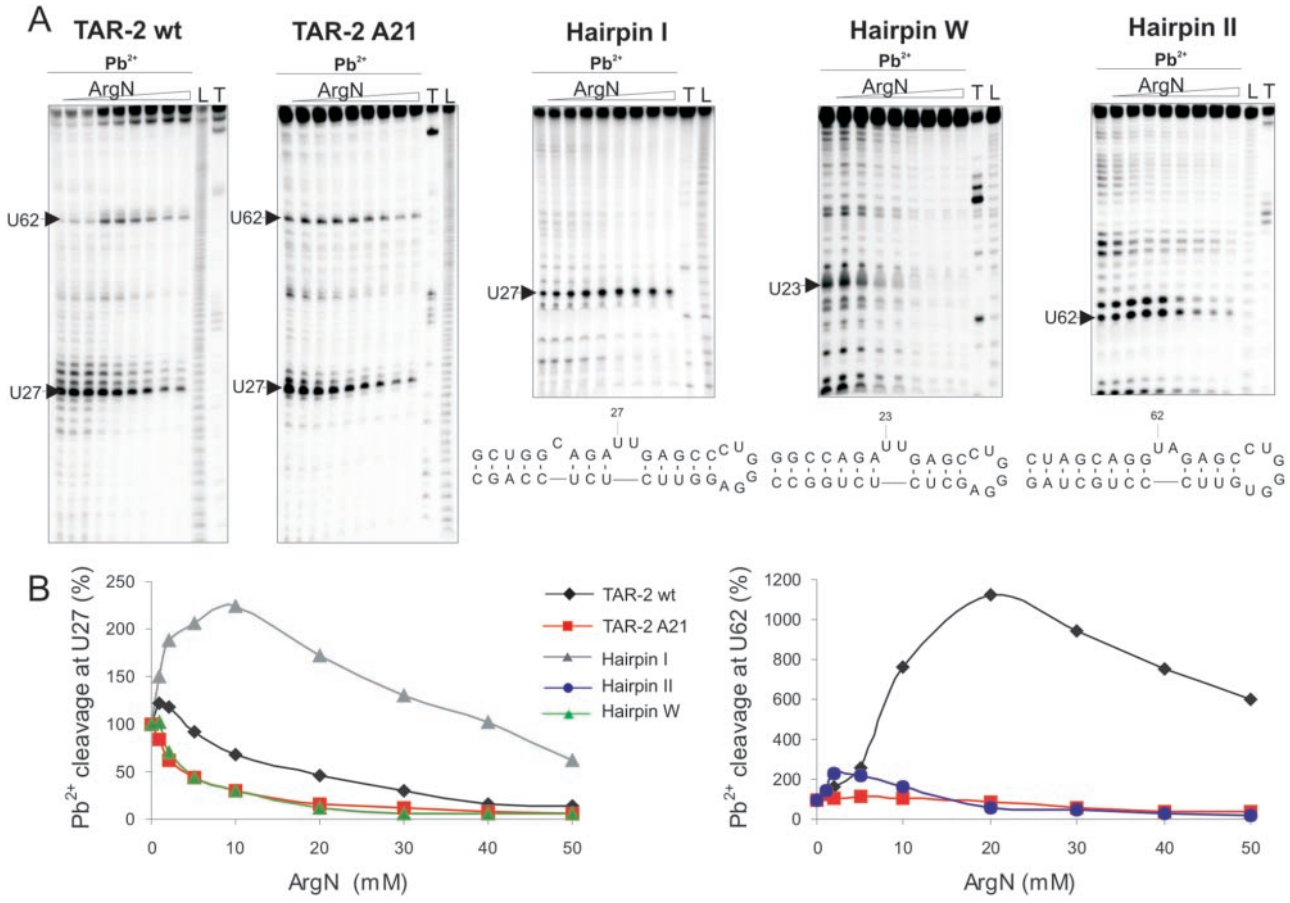

Figure 6. Inhibitory effect of argininamide on Pb^{2+}-induced cleavages. (**A**) Gel patterns are shown for TAR-2 wt, TAR-2 A21 mutant, hairpin I, hairpin W [used in the previous NMR studies, Refs (28,29)] and hairpin II. 2D structures of respective hairpins are presented below gels with cleavage position indicated. Lane L represents formamide ladder; lane T, limited hydrolysis with RNase T1. (**B**) Shows the plot of the argininamide inhibitory effect on the Pb^{2+}-induced cleavages at U27 (U23, as in original report, for the hairpin W) or U62 residues of analysed RNAs.

we found it interesting to note that another type of the pyrimidine-rich internal loop motif, showing Tat-2 binding, was delivered by the *in vitro* RNA selection (46).

CONCLUSIONS

Since the late 1980s, a branched, three-hairpins form was considered as the only representative model of the TAR-2 RNA domain within the HIV-2 leader RNA structure. Here we have shown that the TAR-2 RNA exists *in vitro* in two global, alternative forms: in a new, extended hairpin form, represented by two conformers E1 and E2, and the branched hairpins form. As reflected by the pattern of non-denaturing PAGE gels, the balance between two global TAR-2 forms depends on the concentration of magnesium. The TAR-2 extended form starts to dominate at magnesium concentrations characteristic of the *in vivo* conditions. Mfold-predicted TAR-2 structures, of close energy, have found very good support in the structure probing experimental data despite difficulties resulting from the presence of three TAR-2 conformers at equilibrium. All enzymatic cleavages of the TAR-2 A21 mutant—the mimic of the extended hairpin form—were mirrored for the TAR-2 wt. Furthermore, the existence of the TAR-2 extended form was strongly supported by the enzymatic analysis of the mutants stabilized in the branched form (B4 and ΔC23). Metal ion-induced RNA cleavages appeared instrumental in showing differences between TAR-2 structural forms. The existence of the TAR-2 extended form staying in balance with the branched one strongly points to the structural polymorphism of the 5′ end of the HIV-2 leader RNA. It should be emphasized that the presence of two TAR-1 like hairpins for HIV-2 RNA was always puzzling since it is well-documented that HIV-1 replicates very effectively with only one TAR hairpin. Formation of the TAR-2 extended hairpin form may be taken as an indication of closer than expected overall resemblance between 5′ ends of the HIV-1 and HIV-2 leader RNAs. It remains to be established whether the TAR-2 alternative forms postulated here could be linked with the global conformational changes of the whole HIV-2 leader RNA (4) and play regulatory role in the viral life cycle.

The question arises about the ability to bind Tat-2 protein by the extended hairpin form of the TAR-2 RNA domain. Gel retardation assays reveal that extended form of the TAR-2 binds Tat-2 protein with high affinity. Surprisingly, Tat-2 binds isolated hairpins I and II, the fragments of the TAR-2 branched structure, with low affinity. This allowed us to postulate that the entire tract +18–85, covering sequence of both TAR-2 hairpins I and II, is necessary not only for the architecture of the extended form but also for Tat-2

binding *in vitro*. Applying the argininamide inhibition of Pb^{2+}-induced RNA cleavages we have shown that an internal loop region of the TAR-2 extended hairpin form is a potential Tat-2 binding site. Since the analysis of the branched B4 and ΔC23 mutants gave no conclusive results, our ongoing photochemical experiments will reveal which of the TAR-2 global forms, branched or extended, does offer a preferential binding sites for Tat-2 and cyclin T1.

SUPPLEMENTARY DATA

Supplementary Data are available at NAR Online.

ACKNOWLEDGEMENTS

The authors thank Ben Berkhout for discussion and supplying the HIV-2 Ψ large plasmid with a wild-type HIV-2 ROD DNA sequence, Eliza Wyszko for the Tat-2 plasmid and Mikolaj Olejniczak for preliminary experiments on TAR-2 wt lead cleavages and UV melting. This work was supported by the Foundation for Polish Science (grant SP 01/04) and the Ministry of Education and Science (grant 2P04A06126 and 3 T09A 014 29). Funding to pay the Open Access publication charges for this article was provided by the Ministry of Education and Science grant 3 T09A 014 29.

Conflict of interest statement. None declared.

REFERENCES

1. Rabson,A.B. and Graves,B.J. (1997) Synthesis and processing of viral RNA. In Coffin,J.M., Hughes,S.H. and Varmus,H.E. (eds), *Retroviruses*. Cold Spring Harbor Laboratory Press, Cold Spring Harbor, NY, pp. 205–262.
2. Arya,S.K. and Gallo,R.C. (1988) Human immunodeficiency virus type 2 long terminal repeat: analysis of regulatory elements. *Proc. Natl Acad. Sci. USA*, **85**, 9753–9757.
3. Berkhout,B. and Schoneveld,I. (1993) Secondary structure of the HIV-2 leader RNA comprising the tRNA-primer binding site. *Nucleic Acids Res.*, **21**, 1171–1178.
4. Dirac,A.M., Huthoff,H., Kjems,J. and Berkhout,B. (2002) Regulated HIV-2 RNA dimerization by means of alternative RNA conformations. *Nucleic Acids Res.*, **30**, 2647–2655.
5. Berkhout,B. and Jeang,K.T. (1989) *Trans* activation of human immunodeficiency virus type 1 is sequence specific for both the single-stranded bulge and loop of the *trans*-acting-responsive hairpin: a quantitative analysis. *J. Virol.*, **63**, 5501–5504.
6. Rhim,H. and Rice,A.P. (1993) TAR RNA binding properties and relative transactivation activities of human immunodeficiency virus type 1 and 2 Tat proteins. *J. Virol.*, **67**, 1110–1121.
7. Berkhout,B. and Jeang,K.T. (1992) Functional roles for the TATA promoter and enhancers in basal and Tat-induced expression of the human immunodeficiency virus type 1 long terminal repeat. *J. Virol.*, **66**, 139–149.
8. Jones,K.A. and Peterlin,B.M. (1994) Control of RNA initiation and elongation at the HIV-1 promoter. *Annu. Rev. Biochem.*, **63**, 717–743.
9. Garcia-Martinez,L., Ivanov,D. and Gaynor,R. (1997) Association of Tat with purified HIV-1 and HIV-2 transcription preinitiation complexes. *J. Biol. Chem.*, **272**, 6951–6958.
10. Jones,K.A. (1997) Taking a new TAK on Tat transactivation. *Genes Dev.*, **11**, 2593–2599.
11. Wei,P., Garber,M.E., Fang,S., Fischer,W.H. and Jones,K.A. (1998) A novel CDK9-associated C-type cyclin interacts directly with HIV-1 Tat and mediates its high-affinity, loop-specific binding to TAR RNA. *Cell*, **92**, 451–462.
12. Bieniasz,P.D., Grdina,T.A., Bogerd,H.P. and Cullen,B.R. (1999) Analysis of the effect of natural sequence variation in Tat and in cyclin T on the formation and RNA binding properties of Tat-cyclin T complexes. *J. Virol.*, **73**, 5777–57.
13. Richter,S., Cao,H. and Rana,T.M. (2002) Specific HIV-1 TAR RNA loop sequence and functional groups are required for human cyclin T1-Tat-TAR ternary complex formation. *Biochemistry*, **41**, 6391–6397.
14. Reeves,J.D. and Doms,R.W. (2002) Human immunodeficiency virus type 2. *J. Gen. Virol.*, **83**, 1253–1265.
15. Froeyen,M. and Herdewijn,P. (2002) RNA as a target for drug design, the example of Tat–TAR interaction. *Curr. Top. Med. Chem.*, **2**, 1123–1145.
16. Hamy,F., Felder,E.R., Heizmann,G., Lazdins,J., Aboul-ela,F., Varani,G., Karn,J. and Klimkait,T. (1997) An inhibitor of the Tat/TAR RNA interaction that effectively suppresses HIV-1 replication. *Proc. Natl Acad. Sci. USA*, **94**, 3548–3553.
17. Turner,J.J., Ivanova,G.D., Verbeure,B., Williams,D., Arzumanov,A.A., Abes,S., Lebleu,B. and Gait,M.J. (2005) Cell-penetrating peptide conjugates of peptide nucleic acids (PNA) as inhibitors of HIV-1 Tat-dependent *trans*-activation in cells. *Nucleic Acids Res.*, **33**, 6837–6849.
18. Aboul-ela,F., Karn,J. and Varani,G. (1996) Structure of HIV-1 TAR RNA in the absence of ligands reveals a novel conformation of the trinucleotide bulge. *Nucleic Acids Res.*, **24**, 3974–3981.
19. Kulinski,T., Olejniczak,M., Huthoff,H., Bielecki,L., Pachulska-Wieczorek,K., Das,A.T., Berkhout,B. and Adamiak,R.W. (2003) The apical loop of the HIV-1 TAR RNA hairpin is stabilized by a cross-loop base pair. *J. Biol. Chem.*, **278**, 38892–38901.
20. Puglisi,J.D., Tan,R., Calnan,B.J., Frankel,A.D. and Williamson,J.R. (1992) Conformation of the TAR RNA-arginine complex by NMR spectroscopy. *Science*, **257**, 76–80.
21. Aboul-ela,F., Karn,J. and Varani,G. (1995) The structure of the human immunodeficiency virus type-1 TAR RNA reveals principles of RNA recognition by Tat protein. *J. Mol. Biol.*, **253**, 313–332.
22. Olsen,G.L., Edwards,T.E., Deka,P., Varani,G., Sigurdsson,S.T. and Drobny,G.P. (2005) Monitoring tat peptide binding to TAR RNA by solid-state ^{31}P–^{19}F REDOR NMR. *Nucleic Acids Res.*, **33**, 3447–3454.
23. Emerman,M., Guyader,M., Montagnier,L., Baltimore,D. and Muesing,M.A. (1987) The specificity of the human immunodeficiency virus type 2 transactivator is different from that of human immunodeficiency virus type 1. *EMBO J.*, **6**, 3755–3760.
24. Selby,M.J., Bain,E.S., Luciw,P.A. and Peterlin,B.M. (1989) Structure, sequence, and position of the stem-loop in tar determine transcriptional elongation by tat through the HIV-1 long terminal repeat. *Genes Dev.*, **3**, 547–558.
25. Fenrick,R., Malim,M.H., Hauber,J., Le,S.Y., Maizel,J. and Cullen,B.R. (1989) Functional analysis of the Tat *trans* activator of human immunodeficiency virus type 2. *J. Virol.*, **63**, 5006–5012.
26. Berkhout,B. (1992) Structural features in TAR RNA of human and simian immunodeficiency viruses: a phylogenetic analysis. *Nucleic Acids Res.*, **20**, 27–31.
27. Rhim,H. and Rice,A.P. (1994) Functional significance of the dinucleotide bulge in stem–loop1 and stem–loop2 of HIV-2 TAR RNA. *Virology*, **202**, 202–211.
28. Brodsky,A.S. and Williamson,J.R. (1997) Solution structure of the HIV-2 TAR-argininamide complex. *J. Mol. Biol.*, **267**, 624–639.
29. Brodsky,A.S., Erlacher,H.A. and Williamson,Jr. (1998) NMR evidence for a base triple in the HIV-2 TAR C-G.C+ mutant-argininamide complex. *Nucleic Acids Res.*, **26**, 1991–1995.
30. Berkhout,B., Gatignol,A., Silver,J. and Jeang,K.T. (1990) Efficient *trans*-activation by the HIV-2 Tat protein requires a duplicated TAR RNA structure. *Nucleic Acids Res.*, **18**, 1839–1846.
31. Garcia-Martinez,L.F., Mavankal,G., Peters,P., Wu-Baer,F. and Gaynor,R.B. (1995) Tat functions to stimulate the elongation properties of transcription complexes paused by the duplicated TAR RNA element of human immunodeficiency virus 2. *J. Mol. Biol.*, **254**, 350–363.
32. Oude Essink,B.B., Das,A.T. and Berkhout,B. (1996) HIV-1 reverse transcriptase discriminates against non-self tRNA primers. *J. Mol. Biol.*, **264**, 243–254.
33. Olejniczak,M., Gdaniec,Z., Fischer,A., Grabarkiewicz,T., Bielecki,L. and Adamiak,R.W. (2002) The bulge region of HIV-1 TAR RNA binds metal ions in solution. *Nucleic Acids Res.*, **30**, 4241–4249.

34. McDowell,J.A. and Turner,D.H. (1996) Investigation of the structural basis for thermodynamic stabilities of tandem GU mismatches: solution structure of (rGAGGUCUC)$_2$ by two-dimensional NMR and simulated annealing. *Biochemistry*, **35**, 14077–14089.
35. Mathews,D.H., Sabina,J., Zucker,M. and Turner,D.H. (1999) Expanded sequence dependence of thermodynamic parameters improves prediction of RNA secondary structure. *J. Mol. Biol*., **288**, 911–940.
36. Zucker,M. (2003) Mfold web server for nucleic acid folding and hybridization prediction. *Nucleic Acids Res*., **31**, 3406–3415.
37. Peattie,D.A. and Gilbert,W. (1980) Chemical probes for higher-order structure in RNA. *Proc. Natl Acad. Sci. USA*, **77**, 4679–4682.
38. Rhim,H., Echetebu,C.O., Herrmann,C.H. and Rice,A.P. (1994) Wild-type and mutant HIV-1 and HIV-2 Tat proteins expressed in *Escherichia coli* as fusions with glutathione S-transferase. *J. Acquir. Immune Defic. Syndr*., **7**, 1116–1121.
39. Dirac,A.M., Huthoff,H., Kjems,J. and Berkhout,B. (2001) The dimer initiation site hairpin mediates dimerization of the human immunodeficiency virus, type 2 RNA genome. *J. Biol. Chem*., **276**, 32345–32352.
40. Sarkar,G., Yoon,H.S. and Sommer,S.S. (1992) Screening for mutations by RNA single-strand conformation polymorphism (rSSCP): comparison with DNA-SSCP. *Nucleic Acids Res*., **20**, 871–878.
41. Mandiyan,V. and Boublik,M. (1990) Structural analysis of the 5′ domain of the HeLa 185 ribosomal RNA by chemical and enzymatic probing. *Nucleic Acids Res*., **18**, 7055–7062.
42. Krzyzosiak,W.J., Marciniec,T., Wiewiorowski,M., Romby,P., Ebel,J.P. and Giege,R. (1988) Characterization of the lead(II)-induced cleavages in tRNAs in solution and effect of the Y-base removal in yeast tRNA Phe. *Biochemistry*, **15**, 5771–5777.
43. Ciesiolka,J., Wrzesinski,J., Gornicki,P., Podkowinski,J. and Krzyzosiak,W.J. (1989) Analysis of magnesium, europium and lead binding sites in methionine initiator and elongator tRNAs by specific metal-ion-induced cleavages. *Eur. J. Biochem*., **186**, 71–77.
44. Ciesiolka,J., Michalowski,D., Wrzesinski,J., Krajewski,J. and Krzyzosiak,W.J. (1998) Patterns of cleavages induced by lead ions in defined RNA secondary structure motifs. *J. Mol. Biol*., **275**, 211–220.
45. Tao,J. and Frankel,A.D. (1992) Specific binding of arginine to TAR RNA. *Proc. Natl Acad. Sci. USA*, **89**, 2723–2726.
46. Rhim,H. and Rice,A.P. (1997) RNAs selected *in vitro* by the HIV-2 Tat Protein. *J. Biomed. Sci*., **4**, 28–34.